Trilepton signals in the inert doublet model

Xinyu Miao,[1,*] Shufang Su,[1,†] and Brooks Thomas[1,2,‡]

[1]*Department of Physics, University of Arizona, Tucson, Arizona 85721 USA*
[2]*Department of Physics, University of Maryland, College Park, Maryland 20742 USA*

In this work, we investigate the prospects for detecting the Inert Doublet Model via the trilepton channel at the LHC. We present a set of representative benchmark scenarios in which all applicable constraints are satisfied, and show that in some of these scenarios, it is possible to obtain a signal at the 5σ significance level or better with integrated luminosity of 300 fb^{-1}.

I. INTRODUCTION

The inert doublet model (IDM) is an extension of the standard model (SM) in which the scalar sector of the model includes, in addition to the Higgs field of the SM, an additional $SU(2)_L$ doublet (the so-called "inert doublet"), which couples only to the Higgs and electroweak gauge sectors of the SM. This additional doublet does not acquire a nonzero vacuum expectation value (VEV); hence the fields of this doublet do not contribute to electroweak-symmetry breaking, nor do they mix with those of the SM Higgs doublet. This model was originally proposed [1] for its applications to neutrino physics. However, the recent observation [2] that the presence of an inert doublet can provide the necessary correction to the oblique S and T parameters [3] to accommodate a heavy Higgs boson, with a mass as high as 400–600 GeV, without running afoul of LEP constraints [4] has stimulated a great deal of renewed interest in the model. Since then, the IDM has found a host of additional applications to subjects as diverse as neutrino physics [5], electroweak-symmetry breaking [6], and grand unification [7]. Furthermore, the model is also interesting from the point of view of dark-matter phenomenology. Since an additional discrete symmetry is needed in order to forbid the coupling of the inert doublet to SM fermions, the lightest physical degree of freedom in the inert doublet, if electrically neutral, is a viable weakly interacting massive particle (WIMP) dark-matter candidate. Analyses of the relic abundance of this particle, often referred to as the lightest inert particle (LIP), have been performed [8,9], and assessments of both direct [10] and indirect (including neutrino [11], cosmic-ray positron and antiproton [12], and γ-ray [13]) detection prospects have been carried out.

Given the myriad implications and applications of this model, it is natural to examine how an inert doublet might be identified at the LHC. Certain potential signatures were discussed in [2], and a parton-level analysis of some of these signatures (including a potentially observable modification of the total width of the SM Higgs boson) was performed in Ref. [14]. In Ref. [15], a detailed, detector-level analysis of the detection prospects in the dilepton channel—perhaps the most promising channel in which to search for evidence of an inert doublet at the LHC—was performed for a set of representative benchmark points, each corresponding to a particular region of model parameter space in which the LIP was able to account for the observed dark-matter relic abundance. This analysis showed that an observable signal in this channel could be obtained at the LHC with 100 fb^{-1} of integrated luminosity in a substantial number of these cases. In certain regions of the model parameter space, additional channels, such as $gg \rightarrow AA \rightarrow 4\ell + \not{E}_T$ [16], can also be relevant for discovery.

Since a great many scenarios for physics beyond the standard model (BSM) also give rise to a $\ell^+\ell^- + E_T$ signature, it is worthwhile to investigate other channels which might also yield observable signals indicating the presence of an inert doublet. In this work, we focus on the detection prospects in the trilepton channel: $\ell^+\ell^-\ell^\pm + E_T$. Indeed, this channel has long been regarded as one of the most promising channels in which to look for evidence of physics beyond the standard model, and, in particular, of supersymmetry [17], due to its relatively small SM background.

We begin in Sect. II with a brief review of the inert doublet model and a summary of the relevant theoretical and experimental constraints. We then present a set of benchmark scenarios in which all of these constraints are satisfied and the LIP relic density accounts for the dark matter abundance observed by WMAP [18]. In Sect. III, we discuss trilepton production in the IDM and outline the event-selection criteria we use to differentiate the trilepton signal from the SM background. In Sect. IV, we present our numerical results and discuss the LHC discovery potential for each of our benchmark scenarios, and in Sect. V, we offer some concluding remarks on the scope and implications of our results.

---
*miao@physics.arizona.edu
†shufang@physics.arizona.edu
‡brooks@physics.arizona.edu

II. MODEL PARAMETERS AND BENCHMARK POINTS

The inert doublet model is an extension of the SM in which the fundamental scalar sector comprises not one, but two scalar doublets, which we denote ϕ_1 and ϕ_2. The first of these doublets, ϕ_1, can be identified with the usual Higgs doublet of the SM. It receives a nonzero VEV of $\langle\phi_1^0\rangle = v/\sqrt{2} = 174$ GeV, and consequently bears full responsibility both for electroweak-symmetry breaking (EWSB) and for the generation of SM fermion masses. By contrast, the second doublet, ϕ_2, does not contribute to electroweak-symmetry breaking ($\langle\phi_2^0\rangle = 0$); furthermore, it is prohibited from coupling to the quarks and leptons of the SM by a $\mathbb{Z}_2$ parity (often called matter parity) under which ϕ_2 is odd, whereas all other fields in the theory (including ϕ_1) are even.[1] This $\mathbb{Z}_2$ symmetry also renders the lightest physical degree of freedom contained in ϕ_2— the so-called lightest inert particle, or LIP—absolutely stable, and hence (if neutral) a good WIMP dark-matter candidate.

The most general CP-invariant scalar potential which respects both $SU(2)_L \times U(1)_Y$ gauge-invariance and the aforementioned $\mathbb{Z}_2$ matter parity may be written in the form

$$V = \mu_1^2|\phi_1|^2 + \mu_2^2|\phi_2|^2 + \lambda_1|\phi_1|^4 + \lambda_2|\phi_2|^4$$
$$+ \lambda_3|\phi_1|^2|\phi_2|^2 + \lambda_4|\phi_1^\dagger\phi_2|^2$$
$$+ \left[\frac{\lambda_5}{2}(\phi_1^\dagger\phi_2)^2 + \text{h.c.}\right]. \qquad (1)$$

After EWSB is triggered by the VEV of ϕ_1, the physical scalar spectrum of the model comprises the usual SM Higgs field h (the neutral, CP-even degree of freedom in ϕ_1), as well as four additional fields corresponding to the 4 degrees of freedom in ϕ_2. These include a pair of charged scalars $H^\pm$, a neutral, CP-even scalar S, and a neutral, CP-odd scalar A. The masses of these scalars, written in terms of the parameters appearing in Eq. (1) and the SM Higgs VEV v, are given by

$$m_h^2 = 2\lambda_1 v^2, \qquad (2)$$

$$m_{H^\pm}^2 = \mu_2^2 + \lambda_3 v^2/2, \qquad (3)$$

$$m_S^2 = \mu_2^2 + (\lambda_3 + \lambda_4 + \lambda_5)v^2/2, \qquad (4)$$

$$m_A^2 = \mu_2^2 + (\lambda_3 + \lambda_4 - \lambda_5)v^2/2. \qquad (5)$$

It is also useful to define a pair of mass splittings $\delta_1 \equiv m_{H^\pm} - m_S$ and $\delta_2 \equiv m_A - m_S$. Indeed, for our present purposes, it is most convenient to characterize a given

model in terms of the parameter set $\{m_h, m_S, \delta_1, \delta_2, \lambda_2, \lambda_L\}$, where $\lambda_L \equiv \lambda_3 + \lambda_4 + \lambda_5$ represents the combination of the λ_i in Eq. (1) which controls the size of the hSS and $hhSS$ couplings.

The parameter space of the IDM is restricted by a number of considerations. These include model-consistency requirements, such as perturbativity and vacuum stability, as well as experimental constraints derived from electroweak precision data, the results of direct searches at LEP [20] and at the Tevatron, etc. In addition, if we further demand that the LIP be the dominant component of the dark matter, we must also require that its relic density falls within the WMAP 3σ bounds [18] on the observed dark-matter relic density, and that the appropriate constraints from dark-matter direct-detection experiments are likewise satisfied. Since these constraints, along with their implications for the parameter space of the IDM, have been analyzed and discussed in detail in Refs. [9,15], we will not recapitulate the analysis here, but simply summarize the results. Note that in our analysis below, we will assume that the CP-even scalar S is the dark-matter candidate. The corresponding results obtained in the case in which A plays the role of the dark-matter candidate are very similar.

A number of IDM parameter-space regimes exist in which all of the aforementioned physical constraints are satisfied, and in which the LIP can account for the observed dark-matter abundance. In the first of these regimes, dubbed the "LH" or "light-Higgs" regime, the SM Higgs mass lies within the 114 GeV $\lesssim m_h \lesssim$ 186 GeV preferred by LEP constraints, and electroweak precision data require that δ_1 and δ_2 be of roughly the same order. Here, the LIP is light enough, with a mass in the range 35 GeV $\lesssim m_S \lesssim$ 80 GeV, that its relic abundance is not washed out by $SS \rightarrow WW^{(*)}$ annihilation.

A number of benchmark points corresponding to different possible scenarios within this regime were defined in Ref. [15]. These were specifically chosen with the dilepton channel in mind. The parameter assignments for some of those points, labeled LH1–LH3, are listed in Table I. LH1 and LH2 represent scenarios in which the mass of the dark-

TABLE I. A list of benchmark points used in our analysis, defined in terms of the model parameters $\{m_h, m_S, \delta_1, \delta_2, \lambda_L\}$. Dark matter relic density and collider phenomenology of the IDM depend little on λ_2, which is set to 0.1 for all benchmark points in this study.

Benchmark	m_h (GeV)	m_S (GeV)	δ_1 (GeV)	δ_2 (GeV)	λ_L
LH1	150	40	100	100	−0.275
LH2	120	40	70	70	−0.15
LH3	120	82	50	50	−0.20
LH6	130	40	100	70	−0.18
LH7	117	37	70	100	−0.14
LH8	120	78	70	35	−0.18

---

[1]Such discrete symmetries arise naturally in a variety of theoretical frameworks. For a motivation in the context of grand unified theories, see, for example, Ref. [19].

matter candidate is light ($m_S \sim 40$ GeV), and in which the relationships between M_W, M_Z, and the mass splittings δ_1 and δ_2 are given by $\delta_1 = \delta_2 > M_{W,Z}$ and $\delta_1 = \delta_2 < M_{W,Z}$ for point LH1 and LH2, respectively. Since the contributions from the SM background (and consequently the event-selection criteria we impose) differ significantly depending on whether the W and Z bosons during the decays of the inert scalars are on- or off-shell, we also incorporate two more benchmark points into our analysis. These points, which we dub LH6 and LH7, respectively, represent the situations in which $\delta_1 > M_W$, with $\delta_2 < M_Z$; and $\delta_1 < M_W$, with $\delta_2 > M_Z$. Benchmarks LH3 and LH8 represent scenarios in which the mass of the dark-matter candidate is roughly $m_S \sim 80$ GeV, and in which both δ_1 and δ_2 are restricted to be lighter than M_W. LH3 represents the case in which $\delta_1 \sim \delta_2$, while LH8 represents the case when $\delta_1 > \delta_2$. The latter case has been included primarily as it exemplifies the case in which $SH^\pm$ pair production, with $H^\pm \to AW^{\pm*} \to SZ^*W^{\pm*}$, also contributes to the trilepton signal. Note that points LH6–LH8 have been included (in addition to the benchmark points defined in Ref. [15]) to highlight the effect of relationships between model parameters (primarily δ_1 and δ_2) which have little effect on results in the dilepton channel (the results in which are fairly insensitive to the value of δ_1), but have a substantial effect on results in the trilepton channel. The additional benchmark points LH4 and LH5, defined in Ref. [15], have been left out of this analysis, since each of those two points involves a value of either δ_1 or δ_2 so small (10 GeV) that the vast majority of final-state leptons will escape detection, rendering a trilepton signal essentially unobservable at the LHC.

In the second parameter-space regime in which the IDM successfully accounts for the observed dark-matter abundance, which we dub the ''HH'' or ''heavy-Higgs'' regime, the Higgs mass lies within the range 400 GeV $\lesssim m_h \lesssim 600$ GeV. In this case, electroweak-precision constraints require that $\delta_1 \gg \delta_2$, with δ_1 typically larger than 150 GeV. Consequently, the charged scalars $H^\pm$ tend to be quite heavy. In addition, in order to satisfy the WMAP constraint on the dark-matter density, the LIP mass must be $m_S \approx 75$ GeV. While the prospects for detecting a dilepton signature in such scenarios can be quite good [15], depending primarily on whether or not $\delta_2 < M_Z$, a trilepton signature proves far more difficult to detect. The reason for this is that the primary source of observable dilepton events in the IDM is the pair-production process $pp \to SA$, the cross section for which is independent of δ_1. By contrast, the primary source for an observable trilepton signal, as will be discussed in more detail below, is $pp \to H^\pm A$, which depends on both δ_1 and δ_2. The cross section for this process is therefore substantially suppressed due to the large value of δ_1. Consequently, in what follows, we will focus primarily on the detection prospects for the light-Higgs scenarios alone.

In addition to these two cases, a number of other parameter-space regimes exist in which all constraints are satisfied, and in which the LIP relic density reproduces the observed dark-matter relic density [9]. However, these scenarios do not yield observable signals in either the dilepton or trilepton channel, generally, either because all of the inert scalars are required to be extremely heavy, or else because δ_2 is required to be quite small ($\delta_2 \lesssim 30$ GeV), and hence the charged leptons resulting from A decay are extremely soft. We will therefore not consider the collider phenomenology of such models further here, but we emphasize that they are still viable scenarios.

III. TRILEPTON PRODUCTION IN THE INERT DOUBLET MODEL

A number of processes contribute to the overall trilepton signal in the IDM. Here, we will concentrate on the most promising contributions for detection: those in which one lepton is produced via $W^{(*)}$ decay and the other two via $Z^{(*)}$ decay. The most significant such contributions are

(a) $q\bar{q}' \to AH^\pm$ with $A \to SZ^{(*)} \to S\ell^+\ell^-$ and $H^\pm \to SW^{\pm(*)} \to S\ell\nu$;

(b) $q\bar{q}' \to SH^\pm$ with $H^\pm \to AW^{\pm(*)} \to A\ell\nu$ and $A \to SZ^{(*)} \to S\ell^+\ell^-$,

the corresponding Feynman diagrams for which are shown in Fig. 1. Note that in our analysis, we will consider the case in which $\ell = e$, μ only.

Process (a) will occur in any IDM scenario in which the S plays the role of the LIP, whereas process (b) will occur only in scenarios in which $\delta_1 > \delta_2$ and will only be sizeable when $\delta_1 < M_W$ or $\delta_1 > \delta_2 + M_W$. For all the benchmark points listed in Table I, process (b) is sizable only for LH8. Even in that case, it is subdominant compared to process (a), the overall cross section for which (taking into account all relevant decay branching ratios) is a factor of 20 larger than that for process (b). In cases in which $\delta_2 > \delta_1$, the process $q\bar{q}' \to AH^\pm$, with $A \to H^\pm W^{\mp(*)} \to H^\pm \ell\nu$ and $H^\pm \to SW^{\pm(*)} \to S\ell\nu$, also contributes to trilepton production. The leptons produced in this process all come from $W^{(*)}$ decay, and for this reason, it is difficult to resolve this process from the SM background. For all the benchmark points that we have selected for our study,
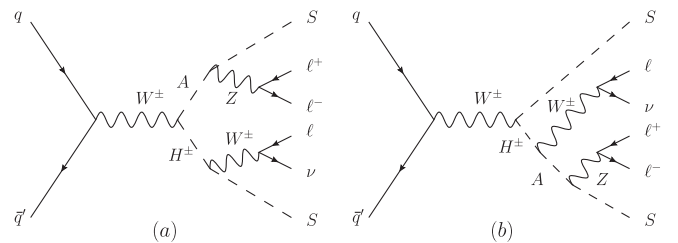

FIG. 1. Diagrams corresponding to the processes which provide the leading contributions to the $\ell^+\ell^-\ell^\pm + E_T$ cross section in the IDM.

however, the overall cross section for this process is negligibly small, and can therefore be safely neglected.

Results for the LHC production cross sections for the dominant ($pp \rightarrow AH^{\pm}$) signal process at $\sqrt{s} = 14$ TeV, as well as the branching fractions for $H^{\pm} \rightarrow S\ell^{\pm}\nu$ and $A \rightarrow S\ell^+\ell^-$ decay, are provided in Table II. Note that for benchmark point LH8, the subdominant contribution to the trilepton signal from $pp \rightarrow SA^{\pm}$ has also been included in our analysis.

A number of processes contribute to the SM background for trilepton production. The most important of these is the irreducible background from WZ/γ^* production, though a number of reducible backgrounds also contribute. One particularly important irreducible background results from $t\bar{t}$ and Wt events (including those involving additional jets) in which both W bosons present after the decay of the top quark(s) decay leptonically, and an additional charged lepton results from the semileptonic decay of a b quark. We will refer to such processes, respectively, as $t\bar{t}(j)$ and $Wt(j)$. Additionally, heavy-flavor processes such as $b\bar{b}Z/\gamma^*$ and $c\bar{c}Z/\gamma^*$, can also be an important background, as recently emphasized in [21], as can $ZZ \rightarrow \ell^+\ell^-\ell^+\ell^-$ events in which one of the charged leptons goes undetected.

In our analysis, event samples both for the signal process and for these backgrounds were generated at parton-level using the MadGraph/MadEvent (version 4.4.32) [22] package. These events were subsequently passed through PYTHIA (version 6.4.14) [23] for parton showering and hadronization, and then through PGS4 [24] to simulate the effects of a realistic detector. The one exception involves the background from heavy-flavor processes, which is somewhat cumbersome to analyze numerically, given the amount of data required to obtain a statistically reliable sample. However, as has been shown in Ref. [21], this background can be effectively eliminated via the implementation of a stringent missing energy cut of order $E_T > 50$ GeV. A similarly stringent cut on the total-transverse-momentum variable H_T should also be quite effective in this regard. We shall therefore assume that these backgrounds are effectively eliminated by the E_T and H_T cuts included among our event-selection criteria.

The $t\bar{t}(j)$ background sample used in our analysis consists of a matched sample of $t\bar{t}$ and $t\bar{t} + 1$ jet events. Matching was carried out at the MadGraph/MadEvent level, according to M. L. Mangano's (MLM) matching scheme, using a K_T jet algorithm (for details, see [25]). Our $Wt(j)$ background was generated in an analogous manner, and includes a pair of matched samples: one consisting of $W^+\bar{t}$ and $W^+\bar{t} + 1$ jet events, the other of W^-t and $W^-t + 1$ jet events. We find that the trilepton results obtained from these samples agree with those obtained by the CMS collaboration [26] to within 10% when similar event-selection criteria are applied.

Let us now turn to discuss those event-selection criteria, which we apply in three successive stages or sets, in more detail. The first set of cuts we impose (hereafter to be referred to as our Level I cuts) is designed to mimic a realistic detector acceptance. More specifically, we require:

(i) Exactly three charged leptons (either electrons or muons), including one same-flavor, opposite-sign (SFOS) pair.

(ii) $p_T^\ell > 15$ GeV and $|\eta_\ell| < 2.5$ for each of these leptons.

(iii) For lepton isolation, we require $\Delta R_{\ell\ell} > 0.4$ for each possible charged-lepton pairing, and $\Delta R_{j\ell} > 0.4$ for each combination of one jet and one charged lepton.

Our second set of cuts (hereafter referred to as our Level II cuts) is designed to suppress reducible backgrounds from SM processes which involve either hard jets or little missing transverse energy:

(i) No jets with $p_T^j > 20$ GeV and pseudorapidity $|\eta| < 3.0$.

(ii) $\not{E}_T > 50$ GeV.

As discussed above, a missing-energy cut of this magnitude effectively eliminates the background from heavy-flavor processes such as $b\bar{b}Z/\gamma^*$ and $c\bar{c}Z/\gamma^*$. The jet veto is quite efficient in reducing background contributions from $t\bar{t}(j)$, $Wt(j)$, and other processes which involve substantial hadronic activity in the central region of the detector. Indeed, after the application of the Level I + II cuts discussed above, the dominant remaining background is the irreducible one from WZ/γ^* production, as shown in Table III. In addition, there is also a non-negligible contribution (amounting to around 5% of the WZ/γ^* background) from residual $t\bar{t}(j)$ and $Wt(j)$ events which survive the jet veto.[2] Other reducible backgrounds, including those from W + jets and heavy-flavor processes, are effectively eliminated by this choice of cuts.

TABLE II. Leading-order cross sections for the associated production of $AH^{\pm}$ at the LHC, with center-of-mass energy $\sqrt{s} = 14$ TeV, for the various benchmark points defined in Table I. The relevant branching fractions of the scalars A and $H^{\pm}$ are also shown.

Benchmark	$\sigma_{AH^{\pm}}$ (fb)	BR($H^{\pm} \rightarrow S\ell^{\pm}\nu$)	BR($A \rightarrow S\ell^+\ell^-$)
LH1	125.2	0.216	0.067
LH2	299.0	0.233	0.068
LH3	154.9	0.233	0.069
LH6	187.0	0.216	0.069
LH7	204.2	0.233	0.067
LH8	159.4	0.226	0.070

---

[2]It should be noted that before the application of any event-selection criteria, our $t\bar{t}(j)$ sample includes 24,200,000 events, of which 752 events survive the Level I + II cuts. This constitutes a statistically sufficient sample.

TABLE III. Cross sections for the signal process $pp \rightarrow AH^{\pm} \rightarrow \ell^+\ell^-\ell^{\pm} + E_T$ in each of the benchmark scenarios presented in Table I, and for the relevant SM backgrounds, after the application of our Level I and Level II cuts.

	Signal			SM Background	
Benchmark	Level I (fb)	Level I + II (fb)	Process	Level I (fb)	Level I + II (fb)
LH1	0.760	0.317	WZ/γ^*	125.767	32.949
LH2	0.817	0.290	$t\bar{t}(j)$	38.869	1.046
LH3	0.289	0.082	$Wt(j)$	1.794	0.536
LH6	0.618	0.239	Total BG	166.430	34.531
LH7	1.089	0.420			
LH8	0.204	0.048			

After the imposition of the Level I and Level II cuts, we impose one further battery of event-selection criteria (hereafter referred to as our Level III cuts). Unlike these first two sets of cuts, which are applied universally to all benchmark points used in this analysis, our Level III cuts are individually tailored to optimize the statistical significance of discovery for each benchmark point. A wide variety of possible criteria could in principle be used in this optimization process; however, we find that one particularly useful criterion that can be used to differentiate between signal and background events is the invariant mass $M_{\ell_Z\ell_Z}$ of the requisite pair of SFOS charged leptons (which we dub ℓ_Z^+ and ℓ_Z^-) that any event must include in order to pass the Level I cuts. If only one SFOS pairing can be constructed for a given event, $M_{\ell_Z\ell_Z}$ is unambiguously defined. In cases in which more than one SFOS combination exists and $\delta_2 \geq 70$ GeV, the pair whose invariant mass is closest to $\min(\delta_2, M_Z)$ will be identified as ℓ_Z^+ and ℓ_Z^-, and that invariant mass will be identified as $M_{\ell_Z\ell_Z}$. In cases in which $\delta_2 < 70$ GeV, the pair whose invariant mass is closest to 70 GeV will be so identified.[3]

The distribution for $M_{\ell_Z\ell_Z}$ peaks around M_Z for the Standard-Model WZ/γ^* background. For the signal process, the peak is around $\min(\delta_2, M_Z)$, as shown clearly in Fig. 2 for LH1 ($\delta_2 = 100$ GeV, left panel) and LH3 ($\delta_2 = 50$ GeV, right panel). This suggests that a cut on $M_{\ell_Z\ell_Z}$ around δ_2 has the potential to suppress significantly the SM background in scenarios in which $\delta_2 < M_Z$. Therefore, in our analysis, we select events on the basis of whether $M_{\ell_Z\ell_Z}$ lies below the threshold

(i) $M_{\ell_Z\ell_Z} \leq M_{\ell_Z\ell_Z}^{\max}$.

In principle, one could also introduce a minimum threshold for $M_{\ell_Z\ell_Z}$, but it turns out that the imposition of such a cut is not particularly helpful in practice; thus we will only make use of the above criterion in what follows.

Furthermore, in cases in which $A \rightarrow S\ell^+\ell^-$ decay occurs via an off-shell Z, the charged leptons will tend to be more collinear than those produced from the decay of an on-shell Z. For this reason, cuts such as

(i) $\cos\phi_{\ell\ell} \geq \cos\phi_{\ell\ell}^{\min}$

(ii) $\Delta R_{\ell\ell} \leq \Delta R_{\ell\ell}^{\max}$,

where $\phi_{\ell\ell}$ is the azimuthal angle between the SFOS lepton pair, can be quite effective in discriminating between signal and background in cases in which $\delta_2 < M_Z$. In practice, we find the $\Delta R_{\ell\ell}^{\max}$ cut alone to be sufficient for our purposes, and thus make use of this criterion exclusively.

From the four-momentum of the remaining lepton (the one that is not part of the $\ell_Z^+\ell_Z^-$ pair), which we dub ℓ_W, we can construct an additional quantity: a transverse-mass variable M_{T_W}, which we define according to the relation

$$M_{T_W}^2 \equiv (E_{\ell_W} + \not{E}_T)^2 - (\vec{p}_{T\ell_W} + \vec{\not{p}}_T)^2, \quad (6)$$

where $\not{E}_T$ and $\vec{\not{p}}_T$ respectively denote the *total* missing transverse energy and missing transverse momentum vector. The distribution for M_{T_W} drops sharply around M_W for the SM WZ/γ^* background. A similar drop also occurs for the signal process, in cases in which the $H^{\pm}$ decays via an on-shell W, but the presence of additional sources of $\not{E}_T$ (the pair of LIPs) in this case results in a smoother M_{T_W} distribution that falls more gently above M_W. In cases in which $\delta_1 < M_W$, and the lepton in question comes from off-shell W decay, the drop in M_{T_W} is quite gradual and occurs near δ_1. The distributions for M_{T_W}, both for the signal process and for the dominant SM backgrounds, are shown in Fig. 3 for LH1 ($\delta_1 = 100$ GeV, left panel) and LH3 ($\delta_1 = 50$ GeV, right panel). The evidence in this figure suggests that in cases in which $\delta_1 > M_W$, imposing a minimum threshold for M_{T_W} can be helpful in reducing the dominant WZ/γ^* background. Conversely, when $\delta_1 < M_W$, an upper limit on M_{T_W} can likewise be of use. Motivated by these considerations, we allow for either a minimum or a maximum threshold for M_{T_W} in our event-selection criteria, and only retain events for which

(i) $M_{T_W} \geq M_{T_W}^{\min}$ or $M_{T_W} \leq M_{T_W}^{\max}$,

depending on the benchmark point in question. As we shall see, such cuts on $M_{\ell_Z\ell_Z}$ and M_{T_W} will turn out to be

---

[3]We choose this criterion for identifying the SFOS pair, rather that simply selecting whichever pair has an invariant mass closer to δ_2. This is because for $\delta_2 \lesssim 70$ GeV, the latter procedure would result in more frequent misidentification of which leptons were produced via Z/γ^* decay in the WZ/γ^* background sample, and consequently lower statistical significance values.
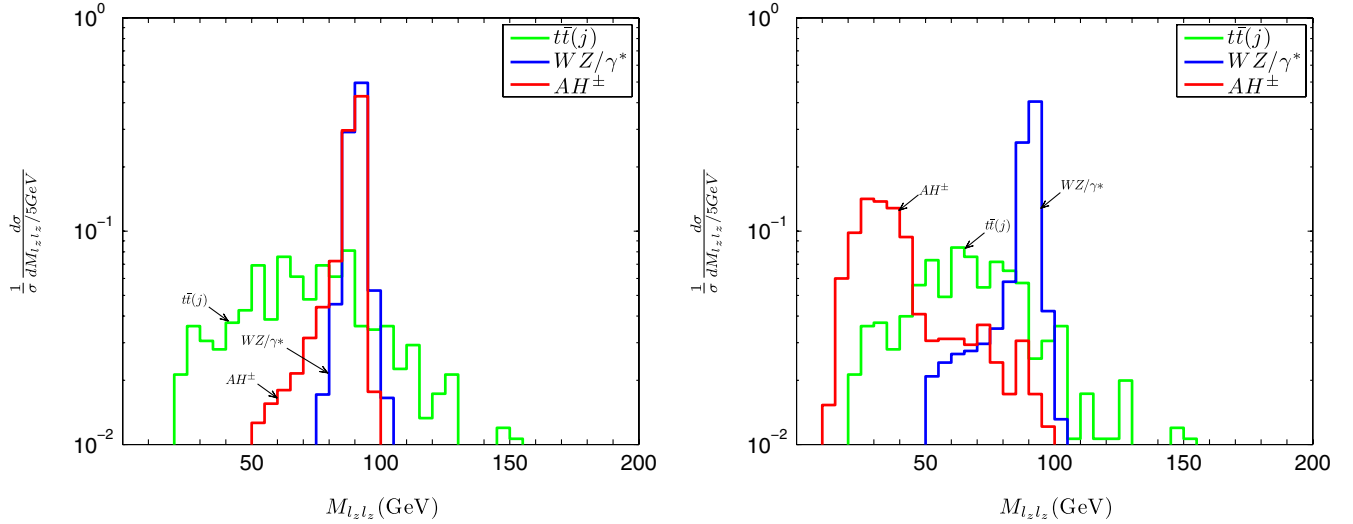
FIG. 2 (color online).   Distributions of the invariant mass of the SFOS lepton pair after the application of the Level I + II cuts described in the text, in our benchmark scenarios LH1 (left panel) and LH3 (right panel), both for the signal process and for the dominant SM backgrounds. Note that the area under each distribution curve has been normalized to one.
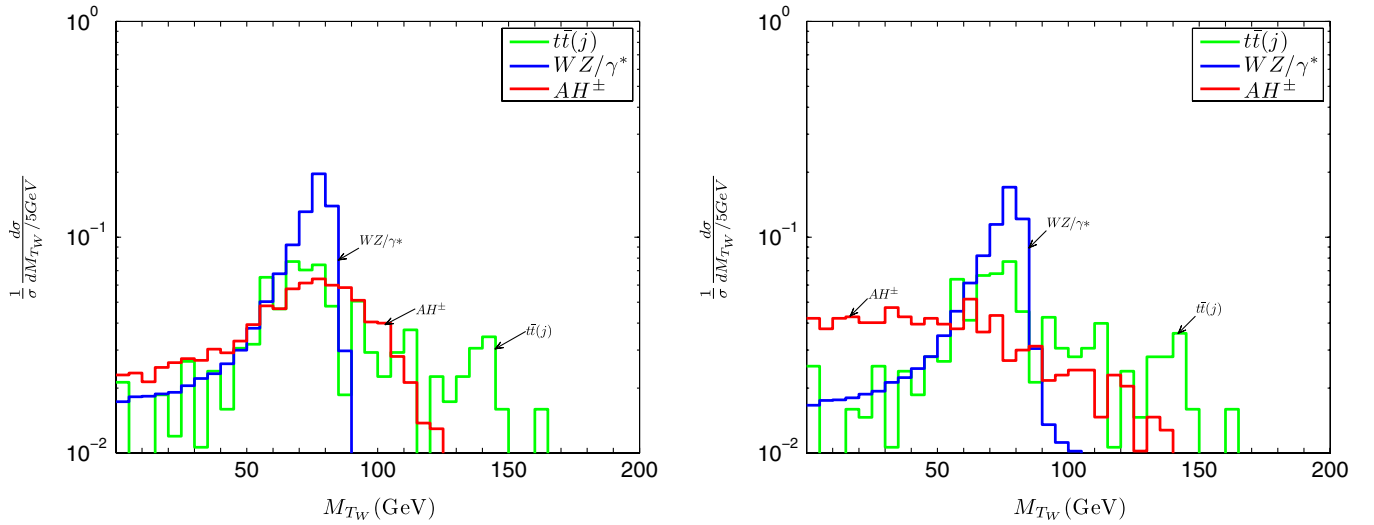

FIG. 3 (color online).   Distributions of the transverse mass variable M_{T_W} defined in Eq. (6), after the application of the Level I + II cuts described in the text, in our benchmark scenarios LH1 (left panel) and LH3 (right panel), both for the signal process and for the dominant SM backgrounds.

particularly useful in distinguishing a trilepton signal from the dominant WZ/γ^* background.

It can also be useful to impose a more stringent lower limit $p_{T_\ell}^{\min}$ on the transverse momentum p_{T_ℓ} of the charged leptons than that imposed at Level I:

  (i) $p_{T_\ell} \geq p_{T_\ell}^{\min} > 15$ GeV.

Likewise, a cut on the total-transverse-momentum variable H_T:

  (i) $H_T \geq H_T^{\min}$,

with H_T defined in terms of the sum

$$H_T = E_T + \sum_{i=1}^{3} |p_{T\ell_i}|, \qquad (7)$$

TABLE IV.   A list of the optimized Level III cuts used in the analysis of each of the benchmark points presented in Table I. An entry of "-" indicates that the corresponding cut is not imposed. For more details on the definition of the thresholds used, see text.

Benchmark	$M_{\ell_z\ell_z}^{\max}$	$M_{T_W}^{\min}$	$M_{T_W}^{\max}$	$\Delta R_{\ell\ell}^{\max}$	$H_T^{\min}$	$p_{T_\ell}^{\min}$
LH1	100 GeV	90 GeV	-	1.6	240 GeV	-
LH2	65 GeV	-	60 GeV	1.3	150 GeV	-
LH3	50 GeV	-	60 GeV	1.2	140 GeV	-
LH6	65 GeV	-	-	1.1	200 GeV	20 GeV
LH7	100 GeV	-	65 GeV	-	200 GeV	-
LH8	40 GeV	-	-	-	-	-

can also be useful in differentiating signal from background. A roster of the particular cuts implemented for each benchmark used in our analysis is compiled in Table IV.

IV. RESULTS

In Table V, we show the discovery potential for the trilepton signal at the LHC (assuming a center-of-mass energy of 14 TeV) for each of the IDM benchmark points defined above, assuming an integrated luminosity of 300 fb^{-1} in each of the two detectors. The best prospects for discovery are obtained for the benchmarks LH2 and LH6, each of which yields a statistical significance of more than 5σ. The reason why these benchmarks are comparatively auspicious is twofold. First, both involve a light LIP, with a mass $m_S \sim 40$ GeV. Second, both also feature a mass splitting $\delta_2 \sim 70$ GeV, which, on the one hand, is small enough that $A \to SZ \to S\ell^+\ell^-$ decays will occur through an off-shell Z boson, but, on the other hand, is large enough so that the resulting charged leptons will not generally be too soft to escape detection.

For LH7, which features a similarly light LIP, with $m_S \sim 40$ GeV, but for which $(\delta_1, \delta_2) = (70, 100)$ GeV, the primary difficulty in resolving the signal is that the (dominant) WZ/γ^* background cannot be suppressed by applying a Z veto on $M_{\ell_Z \ell_Z}$, since $A \to SZ \to S\ell^+\ell^-$ decays occur via an on-shell Z. Indeed, this two-body decay mode of the A is analogous to what are often referred to as "spoiler" processes in the literature on trilepton signals in weak-scale supersymmetry [17]. Thus, although the signal cross section for LH7 after cuts is relatively large, the unsuppressed standard-model WZ/γ^* background renders discovery via this channel difficult. As for LH1, for which $\delta_{1,2} > M_{W,Z}$, the standard-model WZ/γ^* background can be suppressed by imposing a lower limit on M_{T_W}. The signal cross section, however, is very small after the imposition of this cut, which renders a

discovery via this channel difficult for this benchmark scenario as well.

The discovery prospects for benchmark point LH3 are also less auspicious. One reason for this is that the LIP mass is far heavier in this scenario, and the production cross section is therefore appreciably lower, as indicated in Table II. Another is that since δ_1 and δ_2 are smaller for this benchmark than for LH1 and LH6, the charged leptons will be significantly softer, and more of them will escape detection. For this reason, a proportionally greater reduction in signal events occurs as a result of our detector-acceptance cuts, as can be seen from Table III. For benchmark point LH8, δ_2 is smaller still, and the effect of the Level I cuts even more severe; hence the trilepton signal is even more difficult to resolve.

The cross sections used in this analysis were computed at leading-order (LO). It is therefore reasonable to ask how our results would change once next-to-leading-order (NLO) corrections are included. We now demonstrate that the inclusion of higher-order corrections will not dramatically alter those results. The dominant background for all benchmarks used in our analysis, after optimization cuts are applied, is the irreducible background WZ/γ^*, as indicated in Table V. The NLO K-factor for this process (at $\sqrt{s} = 14$ TeV) was calculated in Ref. [27] to be K = 1.79. An estimate of the corresponding K-factor for the $q\bar{q} \to H^\pm A$ signal process can be obtained from that for the analogous, Drell-Yan contribution to $H^\pm A^0$ production in the context of the minimal supersymmetric standard model (MSSM), with all superpartners heavy and decoupled. This K-factor was computed in Refs. [28] to be K $\approx$ 1.20–1.30. Thus, taking both signal and background K-factors into account, the $S/\sqrt{B}$ results at NLO would be roughly 90–97% of the LO results quoted in Table V. The efficiency of our cuts is not primarily limited by event count in the most promising benchmark scenarios; hence we expect that the overall statistical significance for discovery for these sce-

TABLE V. Cross sections for the signal process $pp \to AH^\pm \to \ell^+\ell^-\ell^\pm + E_T$ and for the dominant SM backgrounds from WZ/γ^*, $t\bar{t}(j)$ and $Wt(j)$ production for each of the benchmark points presented in Table I, after the application of our Level III cuts. The total background cross section is also shown. The last two columns display the signal-to-background ratio S/B, and the statistical significance (as given by $S/\sqrt{B}$) corresponding to an integrated luminosity of $\mathcal{L} = 300 \text{ fb}^{-1}$ in each detector at the LHC (operating at a center-of-mass energy $\sqrt{s} = 14$ TeV), after the application of these same cuts.

| | Level III Cuts | | | | | | |
Benchmark	$\sigma_{H^\pm A}$ (fb)	σ_{WZ/γ^*} (fb)	$\sigma_{t\bar{t}(j)}$ (fb)	$\sigma_{Wt(j)}$ (fb)	σ_{BG}^{comb} (fb)	S/B	$S/\sqrt{B}$ (300 fb^{-1})
LH1	0.038	0.159	0.020	0.011	0.191	0.20	2.15
LH2	0.078	0.073	0.019	0.021	0.114	0.68	5.64
LH3	0.035	0.093	0.023	0.014	0.131	0.27	2.36
LH6	0.101	0.185	0.030	0.007	0.221	0.46	5.27
LH7	0.270	7.137	0.084	0.038	7.259	0.04	2.45
LH8	0.031	0.385	0.144	0.061	0.591	0.05	1.00

narios should not be drastically different at NLO than it is at LO.

A few further remarks comparing and contrasting the trilepton phenomenology of the IDM with that of supersymmetric models are in order. Indeed, the process $pp \rightarrow H^\pm A \rightarrow \ell^+\ell^-\ell^\pm + E_T$, which yields the dominant contribution to the trilepton signal in the IDM is in many ways analogous to the direct chargino-neutralino production process $pp \rightarrow \chi_2^0 \chi_1^\pm$, with $\chi_2^0 \rightarrow \chi_1^0 Z^{(*)} \rightarrow \chi_1^0 \ell^+\ell^-$ and $\chi_1^\pm \rightarrow \chi_1^0 W^{\pm(*)} \rightarrow \chi_1^0 \ell\nu$, where $\chi_{1,2}^0$ are the lightest and second lightest neutralinos and $\chi_1^\pm$ is the lightest chargino. This channel has long been regarded as a promising discovery channel for weak-scale supersymmetry. Indeed, as was shown in [29], for certain opportune regions of parameter space, an observable signal could be obtained with less than 30 fb^{-1} of integrated luminosity at the LHC. More recently, the CMS collaboration, working in the context of minimal supergravity, has indicated that a 5σ discovery of supersymmetry could be achieved in this channel with 30 fb^{-1} of integrated luminosity, provided that the gaugino mass parameter $M_{1/2} \lesssim 180$ GeV [26].

Thus, we see that given similar mass spectra, the discovery prospects for the supersymmetric process are markedly better than those for its IDM counterpart. This is primarily due to the substantial difference—a relative factor of around 16—between the production cross sections for $pp \rightarrow \chi_2^0 \chi_1^\pm$ in the MSSM and $pp \rightarrow AH^\pm$ in the IDM. This difference owes to two important distinctions between the characteristics of the relevant particles in the two models. The first of these is that $\chi_1^\pm$ and χ_2^0 are Weyl fermions, whereas $H^\pm$ and A are real scalars. As a consequence, the cross sections for the corresponding processes in the two models differ by a relative factor of roughly 4 in the high-energy limit (i.e., the limit in which $s \gg m_i^2$, where m_i denotes the mass of any of the particles involved in the interaction). The second relevant distinction is that the scalar doublet ϕ_2 of the IDM is in the fundamental representation of $SU(2)$, whereas the charged and neutral Winos (which, respectively, constitute the dominant components of $\chi_1^\pm$ and χ_2^0 in the relevant region of SUSY parameter space) are in the adjoint representation. This translates into another relative factor of 4 between the corresponding production cross sections. The practical consequence of this result, of course, is that observing a trilepton signal in the IDM is far more difficult than it is in its MSSM analogue. Indeed, we have seen that although the trilepton channel is one of the cleanest channels in which one might hope to discover supersymmetry at the LHC, in the IDM, this channel can only be observed in the region of parameter space in which the LIP is light ($m_S \sim 40$ GeV) and the mass splitting δ_2 is relatively large ($\delta_2 \sim 70$ GeV).

While the above analysis was performed assuming a center-of-mass energy $\sqrt{s} = 14$ TeV, it is also worthwhile to consider how the discovery prospects would differ at an

LHC operating energy of $\sqrt{s} = 10$ TeV. In this case, the $pp \rightarrow H^\pm A$ production cross sections are reduced to roughly 60% of the values given in Table II, while the (generally dominant) WZ/γ^* background drops to roughly 80% of its 14 TeV value. Since signal event count is not generally a limiting factor in event selection, we would expect each of the $S/\sqrt{B}$ values quoted above to drop to roughly 65% of its 14 TeV value at a 10 TeV machine, given identical luminosities and assuming similar cut efficiencies. While this is not an imperceptible reduction, it is by no means a severe one; thus, were our universe in fact to resemble that described by an IDM benchmark scenario such as LH2 or LH6, one would still expect to see evidence of trilepton production from the decays of heavy inert particles at the LHC, even at $\sqrt{s} = 10$ TeV. It is also worth remarking that the trilepton signature considered here is a particularly clean one. Consequently, it can be expected that additional complications (from increased pileup, etc.) which would arise in an ultra-high-luminosity environment (such as that associated with the Super-LHC) would not dramatically alter our results. However, that being said, it may still be necessary to increase the minimum p_T^ℓ threshold discussed in Section III and the p_T^j ceiling used in the jet veto in order to deal with these complications.

V. CONCLUSIONS

The inert doublet model is a simple yet incredibly versatile scenario for physics beyond the standard model. Among its phenomenological advantages is that it provides a viable WIMP dark-matter candidate in the form of the lightest inert particle. In this work, we have investigated the observability of a trilepton signal at the LHC in the inert doublet model. While the first signals of an inert doublet at the LHC are likely to appear in the dilepton channel [15], the observation of a signal in the trilepton channel could provide valuable additional information about the parameter space of the model and assist in distinguishing the IDM from other BSM scenarios which give rise to similar signature patterns. We have shown that at an integrated luminosity $\mathcal{L} = 300$ fb^{-1}, it should be possible to resolve the trilepton signal, provided that the LIP is light ($m_S \sim 40$ GeV), the mass splitting δ_2 lies within the range 50 GeV $\lesssim \delta_2 \lesssim M_Z$, and δ_1 is small enough ($\delta_1 \lesssim 100$ GeV) that $H^\pm A$ production is not drastically suppressed. These criteria coincide with those which lead to the best detection prospects in the dilepton channel as well.

It should be noted, however, that one could only hope to observe a trilepton signal in regions of parameter space in which the Higgs is lighter than around 180 GeV. Although the inert doublet model can certainly accommodate a heavier Higgs boson—indeed, among the model's numerous advantages is its ability to alleviate the little hierarchy problem—the requisite contributions to the oblique T parameter needed for this owe to the existence of a sizeable

mass splitting between $H^\pm$ and S. When this is the case, the $pp \to AH^\pm$ production cross section will be highly suppressed, and the trilepton-signal contribution from this process will consequently be unobservable at the LHC.

It is also interesting to consider how the results discussed above would be modified by the presence of additional inert doublets. For concreteness, let us consider a model with two inert doublets, which we dub ϕ_2 and ϕ_3 (recall from Section II that in our notation, ϕ_1 denotes the usual SM Higgs doublet). Let us consider the most general case in which ϕ_2 and ϕ_3 are rendered "inert" (i.e., prohibited from coupling to the SM fermions) by virtue of their both being odd under the same $\mathbb{Z}_2$ symmetry. In this case, no symmetry prevents the corresponding fields in ϕ_2 and ϕ_3 from mixing; thus the lighter and heavier physical CP-odd scalar mass eigenstates A_ℓ and A_h will, in general, be linear combinations of the CP-odd degrees of freedom A_2 and A_3 contained in ϕ_2 and ϕ_3, the physical charged scalars $H_\ell^\pm$ and $H_h^\pm$ will be linear combinations of $H_2^\pm$ and $H_3^\pm$, etc. Assuming that S_ℓ (the lighter of the two CP-even neutral scalars) still plays the role of the LIP, one can define a pair of parameters $\delta_2^{(\ell)} \equiv m_{A_\ell} - m_{S_\ell}$ and $\delta_2^{(h)} \equiv m_{A_h} - m_{S_\ell}$ analogous to our δ_2, which represent the mass splittings between the respective pseudoscalars and S_ℓ. Likewise, one can define a pair of mass splittings $\delta_1^{(\ell)} \equiv m_{H_\ell^\pm} - m_{S_\ell}$ and $\delta_1^{(h)} \equiv m_{H_h^\pm} - m_{S_\ell}$ analogous to our δ_1.

For cases in which $\delta_2^{(\ell)} \approx \delta_2^{(h)}$ and $\delta_1^{(\ell)} \approx \delta_1^{(h)}$ (perhaps due to some additional symmetry of the action which relates ϕ_2 and ϕ_3), the event topologies for all $H_i^\pm A_j \to \ell^+\ell^- + E_T$, where $i, j = \{\ell, h\}$, will be similar. In particular, all such processes will give rise to similar $M_{\ell_z \ell_z}$ and M_{T_W} distributions. In such cases, then, the total signal cross section after optimization cuts are applied will essentially be a sum of the individual contributions $\sigma_{H_i^\pm A_j}$, and $S/\sqrt{B}$ will scale accordingly. Furthermore, in cases in which δ_2^ℓ, $\delta_2^h > M_Z$, and thus both A_ℓ and A_h decay via an on-shell Z, the $M_{\ell_z \ell_z}$ distributions will also be similar, even if δ_2^ℓ and δ_2^h differ significantly. Consequently, the total cross section will also be a sum of the individual contributions in such cases, provided the M_{T_W} distributions, etc. are likewise similar. However, in cases where the mass splittings differ

significantly, and the peaks in the $M_{\ell_z \ell_z}$ and M_{T_W} distributions resulting from the different signal contributions are separated, this will no longer be true. In such cases, the set of optimization cuts which maximize $S/\sqrt{B}$ can differ drastically from those which maximize this quantity in the case of a single inert doublet, and depend intimately on the details of the model.

In scenarios in which ϕ_2 and ϕ_3 are rendered inert by different symmetries, no mixing between the fields in these doublets is permitted. However, as far as trilepton production is concerned, the collider phenomenology is essentially analogous to the mixed case discussed above, and the results for any given model still depend intimately on its mass spectrum.

As a final word, we note that although the analysis performed in this work was conducted within the framework of the inert doublet model, similar signatures involving the production of charged and neutral scalars which subsequently decay into other, lighter, scalar particles and SM gauge bosons appear in many other BSM scenarios. We emphasize that our results should apply not only to models involving one or more inert doublets, but also in any scenario involving charged or neutral scalars which decay into a lighter scalar particle which is neutral and stable (on collider time scales), and hence appears in the detector as missing energy. The observation of a clean trilepton $+ E_T$ signal above the SM background would be a clear indication of new physics. To determine the precise nature of that new physics, however, and to pin down the particle nature of the dark matter candidate will likely require additional data from a variety of sources. These may include complementary channels at the LHC, signals at direct or indirect dark-matter-detection experiments, or results from one of many other available experimental probes of physics beyond the standard model.

ACKNOWLEDGMENTS

[1] N. G. Deshpande and E. Ma, Phys. Rev. D **18**, 2574 (1978).

[2] R. Barbieri, L. J. Hall, and V. S. Rychkov, Phys. Rev. D **74**, 015007 (2006).

[3] M. E. Peskin and T. Takeuchi, Phys. Rev. D **46**, 381 (1992).

[4] M. W. Grunewald, J. Phys. Conf. Ser. **110**, 042008 (2008).

[5] E. Ma, Phys. Rev. D **73**, 077301 (2006).

[6] T. Hambye and M. H. G. Tytgat, Phys. Lett. B **659** 3, 651 (2007).

[7] M. Lisanti and J. G. Wacker, arXiv:0704.2816.

[8] L. Lopez Honorez, E. Nezri, J. F. Oliver, and M. H. G. Tytgat, J. Cosmol. Astropart. Phys. 02 (2007) 028; L. L. Honorez and C. E. Yaguna, arXiv:1003.3125.

[9] E. M. Dolle and S. Su, Phys. Rev. D **80**, 055012 (2009).

[10] D. Majumdar and A. Ghosal, Mod. Phys. Lett. A **23**, 2011

(2008).

[11] P. Agrawal, E. M. Dolle, and C. A. Krenke, Phys. Rev. D **79**, 015015 (2009).

[12] E. Nezri, M. H. G. Tytgat, and G. Vertongen, J. Cosmol. Astropart. Phys. 04 (2009) 014.

[13] M. Gustafsson, E. Lundstrom, L. Bergstrom, and J. Edsjo, Phys. Rev. Lett. **99**, 041301 (2007).

[14] Q. H. Cao, E. Ma, and G. Rajasekaran, Phys. Rev. D **76**, 095011 (2007).

[15] E. Dolle, X. Miao, S. Su, and B. Thomas, Phys. Rev. D **81**, 035003 (2010).

[16] M. Kadastik, K. Kannike, A. Racioppi, and M. Raidal, arXiv:0912.3797.

[17] R. Arnowitt and P. Nath, Mod. Phys. Lett. A **2**, 331 (1987); H. Baer and X. Tata, Phys. Rev. D **47**, 2739 (1993); H. Baer, C. Kao, and X. Tata, Phys. Rev. D **48**, 5175 (1993); T. Kamon, J. Lopez, P. McIntyre, and J. T. White, Phys. Rev. D **50**, 5676 (1994); H. Baer, C.-h. Chen, C. Kao, and X. Tata, Phys. Rev. D **52**, 1565 (1995); S. Mrenna, G. L. Kane, G. D. Kribs, and J. D. Wells, Phys. Rev. D **53**, 1168 (1996); K. T. Matchev and D. M. Pierce, Phys. Lett. B **467**, 225 (1999); Phys. Rev. D **60**, 075004 (1999).

[18] D. N. Spergel *et al.* (WMAP Collaboration), Astrophys. J. Suppl. Ser. **148**, 175 (2003).

[19] M. Kadastik, K. Kannike, and M. Raidal, Phys. Rev. D **81**, 015002 (2010).

[20] E. Lundstrom, M. Gustafsson, and J. Edsjo, Phys. Rev. D **79**, 035013 (2009).

[21] Z. Sullivan and E. L. Berger, Phys. Rev. D **78**, 034030 (2008).

[22] J. Alwall *et al.*, J. High Energy Phys. 09 (2007) 028.

[23] T. Sjostrand, S. Mrenna, and P. Skands, J. High Energy Phys. 05 (2006) 026.

[24] ''PGS—Pretty Good Simulator'', http://www.physics. ucdavis.edu/~conway/research/software/pgs/pgs4-general.html.

[25] J. Alwall *et al.*, Eur. Phys. J. C **53**, 473 (2008).

[26] G. L. Bayatian *et al.* (CMS Collaboration), J. Phys. G **34**, 995 (2007).

[27] J. Ohnemus, Phys. Rev. D **50**, 1931 (1994).

[28] S. Kanemura and C. P. Yuan, Phys. Lett. B **530**, 188 (2002); Q. H. Cao, S. Kanemura, and C. P. Yuan, Phys. Rev. D **69**, 075008 (2004).

[29] H. Baer, C. h. Chen, F. Paige, and X. Tata, Phys. Rev. D **50**, 4508 (1994).